A Numerical Study on the Principle of Mechanical Softreduction for Reducing the Centerline Segregation in Slab Casting

M. Wu[1*], J. Domitner[2], F. Mayer[2], A. Ludwig[1,2]

[1] Chair of Simulation and Modeling of Metallurgical Processes, Univ. of Leoben, Austria
[2] Christian Doppler Laboratory for Multiphase Modeling of Metallurgical Processes, Univ. of Leoben, Austria
[*] Corresponding author, Franz-Josef-Str. 18, A-8700 Leoben, Austria, email: menghuai.wu@unileoben.ac.at

Abstract. An Eulerian two-phase columnar solidification model is used to study the principle of mechanical softreduction (MSR) for reduction of the centerline segregation in slab casting. Interdendritic flow, the main cause of segregation, is calculated in the two-phase mushy region during solidification. The motion of the solidified shell and solidifying columnar dendrites in response to the mechanical deformation caused by bulging and MSR is modeled according to a modified Miyazawa-Schwerdtfeger-approach [Arch. Eisenhüttenwes, vol. 52, 1981, pp.415]. A benchmark slab (9 m in length) of plain-carbon-steel is considered. Case simulations were made by varying the following parameters: the position of MSR; the reduction rate; the mechanical behavior of the MSR segment, i.e. the elongation or shortening of the MSR segment in casting direction; 'flattening' of the slab surface near the position of crater end. Further insides to the principle of the MSR are gained. With enhanced computation power the current model can be applied for a parameter study on the MSR efficiency of realistic continuous casting processes.

Keywords: steel, continuous casting, slab, soft reduction, macrosegregation, multiphase simulation.

1. Introduction

Although, mechanical softreduction (MSR) has successfully been implemented in industry practice to reduce the centerline/axial segregation in slab and bloom castings [1-6], the control of the MSR process still relies on plant trials. Empirical knowledge has shown that ideal MSR efficiency could be achieved when the MSR is operating at the optimum condition. According to Thome and Karste [3], the optimum MSR is defined by a minimum intensity of reduction which is necessary to compensate shrinkage during solidification but without creating internal cracks. However, implementation of the empirical knowledge in industry praxis is often not straightforward. Depending on the casting format and steel grade, it is found that optimum MSR positions and rates differ significantly from case to case. Better understanding of phenomena occurring during MSR is still needed.

Using a modeling approach to investigate macrosegregation in slab casting due to bulging (mechanical shell deformation) was pioneered by Miyazawa and Schwerdtfeger [7]. Their model was later extended by Kajitani, Drezet and Rappaz [8] to include a more precise calculation of the mechanical deformation between successive rolls (bulging), a larger calculation domain (5 successive roll-pairs) and the effect of softreduction. Recently, the current authors used a two-phase columnar solidification model to study the formation of centerline segregation in slab castings in an extended domain (including 100 bulging roll-pairs) and with more realistic boundary conditions [9-10]. Their modeling results agreed with findings of previous works [7-8] for the case without softreduction.

The current paper is to continue this works by including mechanical softreduction. A parameter study was carried out by varying the intensity and position of the MSR, and the mechanical deformation behavior of the MSR segment in both slab thickness direction and casting direction. The main objective of this study is to elucidate the principle that governs the mechanical softreduction (MSR), and to explore the application potential for optimizing the MSR process.

2. Model description

2.1 Two phase solidification model

The two-phase columnar solidification model is a simplified version of the mixed columnar-equiaxed solidification model published in [11-13], just by ignoring the appearance of the equiaxed phase. Details of the numerical model for the columnar solidification are described elsewhere [14].

Theoretically, solidification shrinkage of the last remaining melt should also be fed, although it occurs deep within the mushy zone where the permeability is very low. In reality micro-pores would form or the deformation of the solid dendritic skeletons would compensate the solidification shrinkage so that no feeding is necessary. However, both pore formation and solid deformation are not explicitly modelled in our approach. To avoid convergence problems for flow at high solid fraction a "simplified porosity model (SPM)" was proposed [9], where the solid phase formed from the last remaining melt is treated as a solid-pore mixture phase with a mixture density equal to liquid density.

2.2 Mechanical deformation due to bulging

In the current work, no thermo-mechanical model is used. Nevertheless, the velocity of the solidified shell and the deformation of the growing dendrites are described following the Miyazawa-Schwerdtfeger-approach [7], whereby some extensions were added in order to consider multiple bulging rolls. The *z*-component of solid velocity, $u_{z,s}$, is considered as constant, and equal to the casting speed, v_{cast}. For the *x*-component of the solid velocity, $u_{x,s}$, more sophisticated situations must be considered (see Fig. 1). For the fully solidified strand shell the *x*-component of solid velocity, $u_{x,s}$, is assumed to be equal to the surface velocity, $u^{b}_{x,s}$. The mushy zone is divided into three sub-domains according to the state of the solidification at the casting centerline: sub-domain I with fully liquid core in the casting center ($f_s^{cent} \le 0.01$), sub-domain II with non-strength core in the casting center ($0.01 < f_s^{cent} \le f_s^{0-strength}$), and sub-domain III with 'rigid' core in the casting center ($f_s^{cent} > f_s^{0-strength}$). For the sub-domain I where the dendrite tips have not yet met at the centerline, it is assumed that the solid dendrites move with the same velocity as that of the fully solidified strand shell. In the sub-domain III, we set $u_x = 0$. In the sub-domain II where the columnar tip fronts have met at the centerline, two regions are distinguished: **A** and **B**. In the region **A**, the *x*-component of the solid velocity, $u_{x,s}$, is set to be equal to the surface velocity of the shell, $u^{b}_{x,s}$. In the region **B**, $u_{x,s}$ is supposed to be reduced from its maximum velocity at the 0-strength isoline ($f_s^{0-strength}$) to zero at the casting center. Whereupon it is assumed that it is more likely that most of the deformation happens near the strand core where the solid volume fraction is the lowest. This is different to the assumption that the deformation happens homogenously across the whole mushy zone as made by previous authors [7-8]. Thus, the following formulation is suggested

$$u_{x,s} = u^{b}_{x,s} - u^{b}_{x,s} \cdot e^{-\varphi_1 \cdot \frac{(f_s - f_s^{cent})}{\left(f_s^{0-strength} - f_s\right)^{\varphi_2}}}, \qquad (1)$$

where the constants $\varphi_1 = 50$ and $\varphi_2 = 0.25$ were chosen to ensure that most of the deformation occurs near the casting centerline [10].

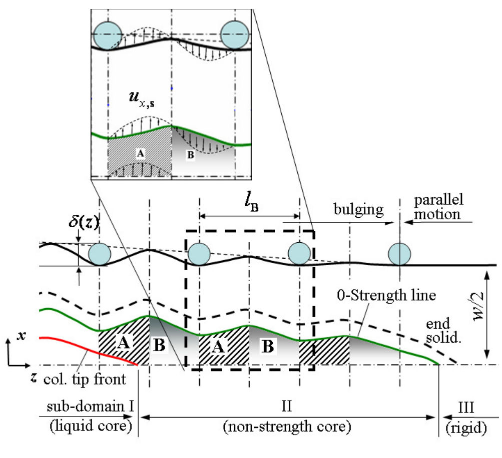

Figure 1. Schematic of the motion of solid shell and growing mushy zone in two phase region.

In order to identify the positions of the columnar tip front, the 0-strength isoline and the end of solidification (Fig. 1) it is assumed that the columnar tip front coincides with $f_s = 0.01$, the 0-strength isoline ($f_s^{0-strength}$) with $f_s = 0.8$ (empirical knowledge from industry praxis) and the end of solidification with $f_s = 0.95$. Here, we also 'switched on' the aforementioned SPM model.

2.3 Mechanical deformation due to softreduction

Deformation of solid phase in the MSR segment is considered in x- and z-direction (Fig. 2), and in the slab width direction it is ignored. In the softreduction segment the strand can deform in thickness direction, and it can also be elongated or shortened in longitudinal (casting) direction. The divergence-free condition for the solid phase ($\nabla \cdot \vec{u}_s = 0$) only applies in regions where the solid fraction is larger than $f_s^{0-strength}$. For solid fraction smaller than $f_s^{0-strength}$ the condition $\nabla \cdot \vec{u}_s = 0$ may be violated, as here deformation of the dendritic skeleton might occur.

Whether the strand in the MSR segment is in compression or tension depends on the z-component velocity of the solid phase at the entrance and exit of softreduction segment, $u^{IN}_{z,s}$ and $u^{OUT}_{z,s}$. Here, $u^{IN}_{z,s}$ is assumed to be equal to the casting velocity, v_{cast}. The section thickness of the strand at the entrance of the softreduction segment is *w*/2 and at the exit it is *w*/2-ε. With a given $u^{IN}_{z,s}$, $u^{OUT}_{z,s}$, *w* and ε, a MSR factor can be defined as:

$$\gamma = \left(u^{OUT}_{z,s} \cdot (w - 2\varepsilon) - u^{IN}_{z,s} \cdot w\right) \cdot \frac{1}{w l_{SR}}. \qquad (2)$$

The MSR factor γ has the same sign and same unit as $\nabla \cdot \vec{u}_s$, and it can actually be understood as a volume averaged divergence of the solid phase over the MSR segment. If γ is zero, it indicates that the divergence-free condition for $\vec{u}_s$ applies to the whole softreduction segment, including the fully solidified region and the solid within the mushy zone. A negative γ means that more solid phase is entering than leaving the softreduction segment (disregard of the solidification in the MSR segment). As the region with solid fraction larger than $f_s^{0-strength}$ is not compressible, γ <1 indicates that the volume compression is only accomplished in the lower solid volume fraction mushy zone. In other words, the interdendritic space between dendrites in the lower solid fraction mushy zone must be reduced, i.e. the dendrites are accumulated (or compressed). The accumulation of the dendrites will squeeze the interdendritic melt out of this region.

On the contrary, a positive γ, corresponding to $\nabla \cdot \vec{u}_s > 0$, means that the interdendritic space in the lower solid fraction region is enlarged, and the melt elsewhere will be sucked into the interdendritic space.

As shown in Fig. 2, we assume no bulging between the roll-pair in the softreduction segment. The surface profile of the strand shell in the softreduction segment is supposed to be linear:

$$x^{\mathrm{b}}(z)=\frac{w}{2}-\frac{\varepsilon}{l_{SR}}\cdot(z-z_1),\qquad(3)$$

where z_1 is the coordinate of the start position of the softreduction segment.

The z-component of the solid velocity in the softreduction segment (including the slab surface) is assumed to vary linearly as:

$$u_{z,\mathrm{s}}=v_{\mathrm{cast}}+\frac{u_{z,\mathrm{s}}^{\mathrm{OUT}}-v_{\mathrm{cast}}}{l_{\mathrm{SR}}}\cdot(z-z_1).\qquad(4)$$

The x-component of the surface velocity of the moving strand is calculated according to $u_{x,\mathrm{s}}^{\mathrm{b}}=u_{z,\mathrm{s}}\cdot dx^{\mathrm{b}}(z)/dz$, and hence

$$u_{x,\mathrm{s}}^{\mathrm{b}}=-\left(v_{\mathrm{cast}}+\frac{u_{z,\mathrm{s}}^{\mathrm{OUT}}-v_{\mathrm{cast}}}{l_{\mathrm{SR}}}\cdot(z-z_1)\right)\cdot\frac{\varepsilon}{l_{\mathrm{SR}}}.\qquad(5)$$

Within the softreduction segment for solid fraction larger than $f_{\mathrm{s}}^{0\text{-strength}}$, where the condition of divergence-free holds we get

$$\frac{\partial u_{x,\mathrm{s}}}{\partial x}=-\frac{u_{z,\mathrm{s}}^{\mathrm{OUT}}-v_{\mathrm{cast}}}{l_{\mathrm{SR}}}.\qquad(6)$$

Integration of Eq.(6) in x direction gives

$$u_{x,\mathrm{s}}=A-\left(\frac{u_{z,\mathrm{s}}^{\mathrm{OUT}}-v_{\mathrm{cast}}}{l_{\mathrm{SR}}}\right)\cdot x,\qquad(7)$$

where the integral constant A is defined by applying the boundary condition, $u_{x,\mathrm{s}}=u_{x,\mathrm{s}}^{\mathrm{b}}$, at the strand surface, $x=x^{\mathrm{b}}(z)$:

$$A=\left(\frac{u_{z,\mathrm{s}}^{\mathrm{OUT}}-v_{\mathrm{cast}}}{l_{\mathrm{SR}}}\right)\cdot\left(\frac{w}{2}-\frac{2\varepsilon}{l_{\mathrm{SR}}}\cdot(z-z_1)\right)-v_{\mathrm{cast}}\cdot\frac{\varepsilon}{l_{\mathrm{SR}}}.\qquad(8)$$

Eq.(7) is used to calculate the solid velocity of the strand shell for solid volume fraction larger than $f_{\mathrm{s}}^{0\text{-strength}}$. In the mushy zone with solid volume fraction less than $f_{\mathrm{s}}^{0\text{-strength}}$, it is distinguished between columnar dendrite trunks moving away from the center and those moving towards the center. For moving outwards, $u_{x,\mathrm{s}}$ is calculated according to Eq.(7). For moving inwards, $u_{x,\mathrm{s}}$ decreases from its maximum velocity at the 0-strength isoline to 0-velocity at the casting centerline according to Eq.(1).

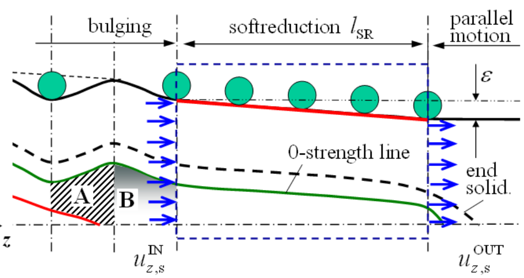

Figure 2. Schematic of softreduction segment.

3. Configuration of the benchmark

A 2D benchmark slab casting of plain-carbon-steel (Fe-0.18 wt.% C) was simulated. The surface profile due to bulging (Fig.3) is described by

$$x^{\mathrm{b}}(z)=\frac{w}{2}+\frac{\delta^{\mathrm{b}}(z)}{2}+\frac{\delta^{\mathrm{b}}(z)}{2}\cdot\sin\!\left(2\pi\frac{z-z_0}{l_{\mathrm{B}}}-\frac{\pi}{2}\right)$$

with $$\delta^{\mathrm{b}}(z)=\delta_{\max}^{\mathrm{b}}+\frac{\delta_{\max}^{\mathrm{b}}}{l_{\mathrm{B}}N}\cdot(z_0-z).\qquad(9)$$

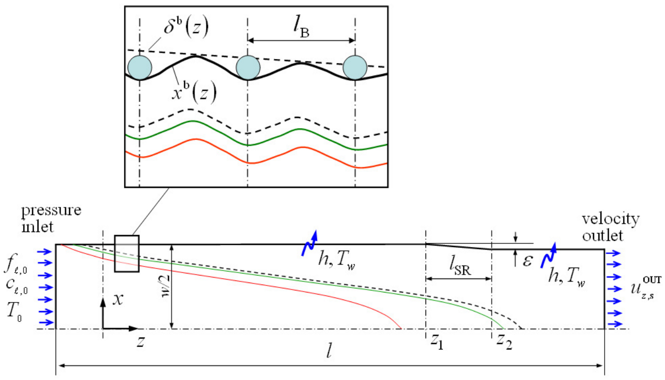

Figure 3. Configuration of the benchmark slab casting.

Table 1. Parameters used for the process simulations

Thermo-physical:	Thermodynamic†:
μ_ℓ = 5.6 x 10^{-3} kg·m^{-1}·s^{-1}	c_{E} = 4.3 wt.%
c_{p}^{ℓ} ($c_{\mathrm{p}}^{\mathrm{s}}$) = 808.25 J·kg^{-1}·K^{-1}	k = 0.36
D_ℓ = 2 x 10^{-8} m^2·s^{-1}	m = -116.7.0 K/wt.%
k_ℓ = 29 W·m^{-1}·K^{-1}	T_{f} = 1811.0 K
k_s = 35 W·m^{-1}·K^{-1}	Δh_f = 2.56 x 10^5 J·kg^{-1}
ρ_ℓ = 7027 kg·m^{-3}	Slab geometry:
ρ_s = 7324 kg·m^{-3}	l = 9 m
Softreduction†:	w = 0.215 m
z_1 = 4.5 m	Boundary conditions†:
z_2 = 6.0 m	$c_{\ell,0}$ = 0.18 wt.%
l_{SR} = 1.5 m	$f_{\ell,0}$ = 1-10^{-5}
ε = 2x10^{-4} m	h = 235 W·m^{-2}·K^{-1}
Rolls and bulging:	T_0 = 1791 K
N = 100	T_w = 325 K
$\delta_{\max}^{\mathrm{b}}$ = 8x10^{-4} m	$u_{z,s}^{\mathrm{IN}}$ = 6.0 x 10^{-3} m·s^{-1}
l_{B} = 0.06 m	$u_{z,s}^{\mathrm{OUT}}$ = 6.0224x10^{-3} m·s^{-1}
z_0 = 0.0 m	

† For parameter study some of them are varied.

The slab is assumed to be casted horizontally. A velocity boundary condition ($u_{z,s}^{\mathrm{OUT}}$) is applied at the outlet, and a pressure boundary condition is applied at the inlet. The heat transfer boundary condition and the casting speed are chosen such that full solidification was gained within the calculation domain under steady-state conditions. The so-called 'modified heat capacity method' from Niyama and co-workers [15] is used to 'adjust' the end of solidification at the desired position, instead of changing the position of the MSR segment. All the parameters used for the process simulations are listed in Table 1.

With this benchmark geometry, a parameter study was carried out by varying the MSR parameters as listed in Table 2. In Case 1 no softreduction was applied. From Case 2 to 7 the same reduction amount ε and same reduction length l_{SR} were applied, but the reduction position $f_{s,Start}^{cent}$ (centerline solid fraction at the starting point of MSR) and the MSR factor γ were varied. From Case 8 to 12 a so-called 'flattening' method is tried, i.e. ε was set to zero but the starting position of flattening ($f_{s,Start}^{cent}$) was varied. As mentioned previously a 'modified heat capacity method' [15] is used to adjust the end of solidification, hence to study the effect of the position of the MSR segment.

Table 2. Parameter study for the softreduction

	MSR parameters				Δc_{mix} *
	l_{SR} (m)	ε (mm)	γ (10^{-6})	$f_{s,Start}^{cent}$	(10^{-4})
Case 1	0	0	0	-	1.4
Case 2	1.5	0.2	-7.44	0.4	2.0
Case 3	1.5	0.2	8.52	0.4	1.5
Case 4	1.5	0.2	0	0.4	0.8
Case 5	1.5	0.2	-15.4	0.4	3.2
Case 6	1.5	0.2	4.52	0.2	0.8
Case 7	1.5	0.2	8.52	0.2	0.8
Case 8	-	0	0	0.5	2.0
Case 9	-	0	0	0.4	0.8
Case 10	-	0	0	0.2	0.7
Case 11	-	0	0	0.1	0.6
Case 12	-	0	0	0.01	0.6

* Difference between maximum & minimum c_{mix} in the solidified slab.

4. Centerline segregation

The simulation result for the Case 1, where no MSR is applied, has been published previously [9-10]. The typical experimentally observed macrosegregation profile across the slab section is numerically predicted (Fig. 4): a positive segregation peak at the casting center accompanied by two negative segregation areas at both sides. The evolution of the macrosegregation along the centerline (Fig. 5) shows the sum-up effect of the series of bulging. The positive segregation peak at the casting center is due to the flow of enriched residual liquid towards the centerline in the region **A**. The negative segregation valleys accompanying the centerline segregation peak is formed in region **B**. Two reasons for the formation of negative segregation in region **B** can be specified: first the residual liquid flows from hot to cold regions (the hot melt entering the volume element contains less solute compared to the cold liquid leaving it); second the solid phase region is compressed. The contributions to the centerline segregation by two different flow mechanisms, namely bulging- and solidification-shrinkage-induced flow were also investigated. Considering only shrinkage-induced feeding flow, the predicted macrosegregation pattern shows negative centerline segregation, while bulging-induced flow induces positive centerline segregation. When the above two flow mechanisms are superimposed the bulging effect dominates over the shrinkage effect.

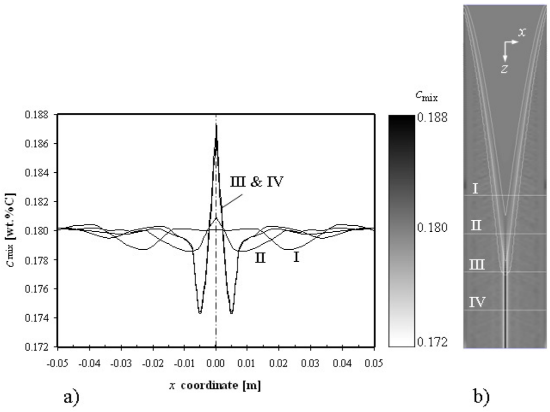

Figure 4. Predicted macrosegregation (c_{mix}) of Case 1. a) c_{mix} profiles across the casting sections at different positions; b) c_{mix} in gray scale: light for negative segregation and dark for positive segregation. The domain is down scaled by 1:10 in z direction.

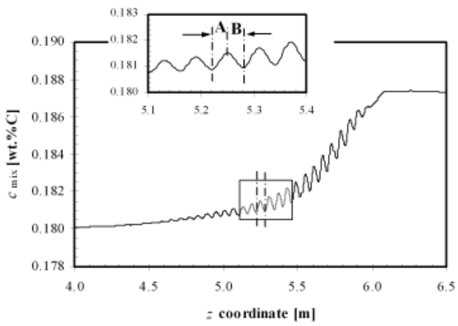

*Figure 5. Evolution of macrosegregation along the casting centerline (Case 1). **A** and **B** indicate the opening and the closing regions between a single roll pair (Fig. 1).*

5. Parameter study

5.1. MSR segment under elongation (Case 3)

For the Case 3, the MSR segment were subject to a reduction rate (ε / l_{SR}) of 1.334 x 10^{-4}. The solid velocity at the entrance and exit of the MSR segment, $u_{z,s}^{IN}$, $u_{z,s}^{OUT}$, were 6.0 x 10^{-3} and 6.0224 x 10^{-3} m·s^{-1}, respectively. Thus, the MSR factor γ results to 8.52 x 10^{-6}, indicating that the MSR segment is in tension. The interdendritic space in the lower solid fraction region ($f_s < f_s^{0-strength}$) is enlarged, and additional melt is needed to feed the enlarged interdendritic space. The solidification shrinkage needs to be fed as well. Therefore, both shrinkage-induced feeding flow and MSR-induced flow are imposed together to enhance the interdendritic flow in the MSR segment.

As shown in Fig. 6(b), the magnitude of the calculated relative velocity $|\Delta \vec{u}_{\ell-s}|$ at the centerline just before the start of MSR (4.455 m from the origin) is 1.28 x 10^{-3} m·s^{-1}. The melt is sucked into the MSR segment. In the Case 1, where no MSR is applied, the magnitude of the relative velocity $\left|\Delta\bar{u}_{\ell-s}\right|$ at the same position is calculated to be only 9.3 x 10^{-4} m·s^{-1}, significantly smaller than for Case 3. The larger relative velocity of Case 3 is caused by the enlarged interdendritic space in the MSR segment which has to be fed. The maximum *x*-component $\left|\Delta u_{x,\ell-s}\right|$ at the same position for the Case 3 is predicted to be 6 x 10^{-5} m·s^{-1}, which is of the same magnitude as for Case 1 (5 x 10^{-5} m·s^{-1}). In region **A** the melt flows towards the casting centerline, while in region **B** the melt flows towards the cold region. As studied previously [9-10], this kind of 'pumping' flow originated from bulging is the main mechanism for the positive centerline segregation in slab casting.

As shown in Fig. 6(c), immediately after the start of MSR, the flow is almost parallel (slightly bending upwards) to the centerline. The magnitude of $\left|\Delta\bar{u}_{\ell-s}\right|$ just after the start of MSR (at 4.515 m from the origin) is 1.23 x 10^{-3} m·s^{-1}, the maximum $\left|\Delta u_{x,\ell-s}\right|$ is 6 x 10^{-6} m·s^{-1}. The small upward *x*-component of the relative velocity together with the strong feeding flow in the casting direction would be expected to reduce c_{mix}. While in the second half of the MSR segment, as shown in Fig. 6(d), the flow bends towards the casting centerline. The magnitude of $\left|\Delta\bar{u}_{\ell-s}\right|$ at 5.94 m from the origin is 2.0 x 10^{-5} m·s^{-1}, and the maximum $\left|\Delta u_{x,\ell-s}\right|$ is 5.0 x 10^{-6} m·s^{-1}. This kind of flow pattern near the last-to-solidify position increases the positive centerline segregation.

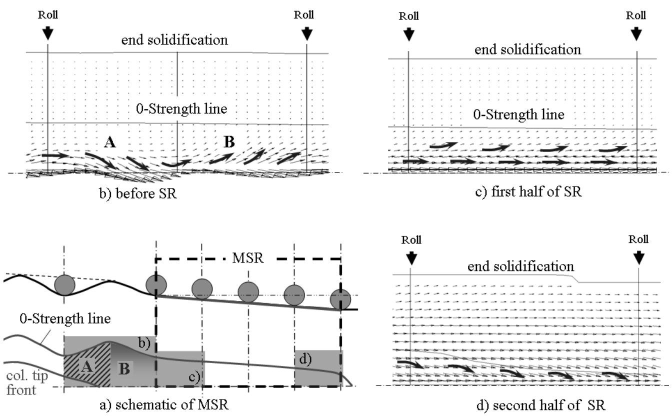

Figure 6. Interdendritic melt flow within the mushy zone for Case 3. a) Schematic of the MSR segment. b)-d) Relative flow fields in different regions as marked in a). Note that the relative velocity is plotted with the x-component being increased by a factor of 10 during post-processing.

The segregation profiles at different cross-sections I) to IV) are shown in Fig. 7. At position I) (before the start of MSR) a typical 'W'-shaped segregation profile can be seen. However, the peak of the centerline segregation is not so high. In section II), located in the first half of MSR segment, the 'W'-shape of the segregation profile remains, but the 'W'-part of the c_{mix} -curve moves downwards. Both the peak and valleys of c_{mix} are smaller than c_0, hence no positive centerline segregation exists at this position. Position III) and IV) are located after the MSR segment. Both c_{mix} -curves are similar. Compared to the position I) and II), they have moved upwards again. Finally, a relatively strong positive segregation peak accompanied by two strong negative segregation valleys is predicted. The deviation of c_{mix} across the slab cross-section (difference between maximum and minimum c_{mix}), Δc_{mix} , for the Case 3 is 1.5 x 10^{-4}, even worse than the Case 1, for which Δc_{mix} =1.4 x 10^{-4}.

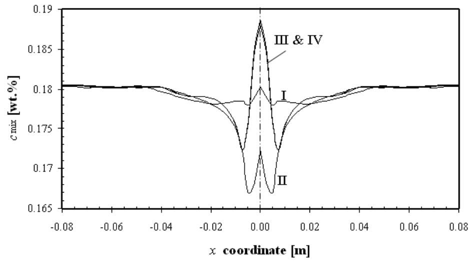

Figure 7. Predicted macrosegregation distribution profiles across different cross-sections for Case 3. The cross-sections I, II, III, IV are at 4, 5, 6, 7 m distance from the origin of the calculation domain.

Fig. 8 shows the evolution of macrosegregation along the casting centerline. Firstly, due to the bulging-induced 'pumping' flow, positive segregation is developing periodically. At the beginning of the MSR segment, c_{mix} is significantly reduced, and even negative centerline segregation is obtained. Starting about 5.1 m from the origin, c_{mix} at the centerline tends to increase again. The slope of the c_{mix} curve in the second half of the MSR segment is quite large and a relatively large positive c_{mix} peak at the casting center is regretfully established again.

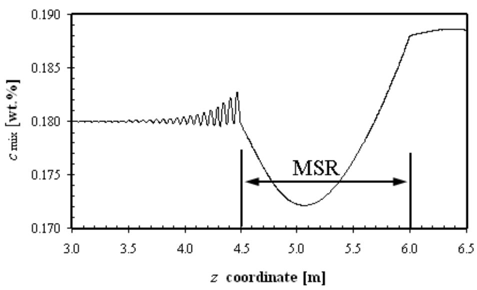

Figure 8. Evolution of macrosegregation along the casting centerline (Case 3).

5.2. MSR segment in compression (case 5)

For Case 5, the same MSR rate as in Case 3 is applied, but the MSR factor is now negative, which means that the solid velocity at the entrance is larger than that at the exit of the MSR segment ($u_{z,s}^{\text{IN}}$ = 6.0 x 10^{-3} m·s^{-1} and $u_{z,s}^{\text{OUT}}$ = 5.989 x 10^{-3} m·s^{-1}). In consequence, the interdendritic space in the lower solid fraction region ($f_s < f_s^{0-\text{strength}}$) is reduced and some interdendritic melt is squeezed out of the MSR segment. Therefore, a backward flow is anticipated. However, solidification shrinkage needs to be fed and thus the backward flow may partially be compensated.

As shown in Fig. 9(b), the magnitude of $|\Delta\bar{u}_{\ell-s}|$ just before the start of MSR (4.455 m from the origin) is 6.0 x 10^{-4} m·s^{-1}. As expected, a backward flow is predicted. The highly solute-enriched melt is squeezed out of the MSR segment. The maximum $|\Delta u_{x,\ell-s}|$ for the Case 5 is predicted to be 5.5 x 10^{-5} m·s^{-1}, which is in the same magnitude as in Case 3 (6 x 10^{-5} m·s^{-1}). In region **A** the melt flows towards the casting centerline, while in region **B** some melt flows towards away from the center. This kind of 'pumping' flow due to bulging induces a 'W'-shaped segregation profile.

As shown in Fig. 9(c), in the first half of the MSR segment the flow is also backward and almost parallel (slightly bending upwards) to the centerline. The magnitude of $|\Delta\bar{u}_{\ell-s}|$ just after the start of MSR (at 4.515 m from the origin) is 2 x 10^{-4} m·s^{-1}, the maximum $|\Delta u_{x,\ell-s}|$ is 3 x 10^{-6} m·s^{-1}. In the second half of MSR, as shown in Fig. 9(d), the relatively large backward flow remains. The magnitude of $|\Delta\bar{u}_{\ell-s}|$ at 5.94 m from the origin is 1.1 x 10^{-4} m·s^{-1}, and the maximum $|\Delta u_{x,\ell-s}|$ is 3.0 x 10^{-5} m·s^{-1}.

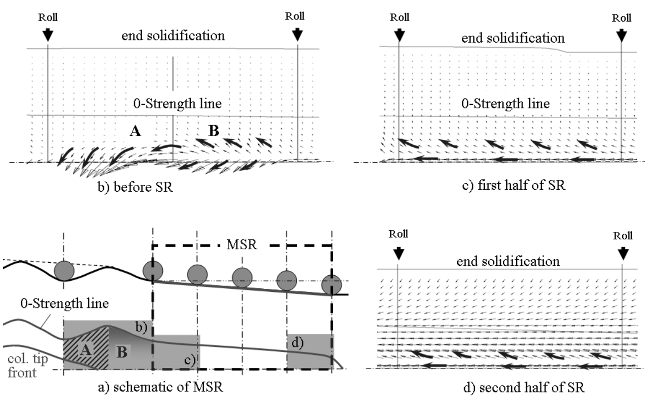

Figure 9. Interdendritic melt flow in the mushy zone for Case 5. a) Schematic of the MSR segment. b)-d) Relative flow fields in different regions as marked in a). Note that the relative velocity is plotted with the x-component being increased by a factor of 10 during post-processing.

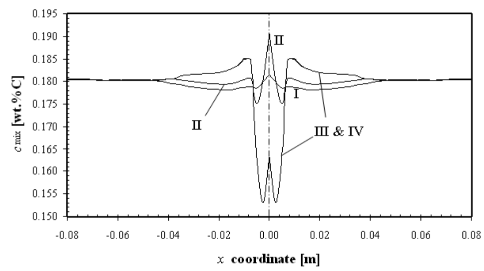

Figure 10. Predicted macrosegregation distribution profiles across different cross-sections for Case 5. The cross-sections I, II, III, IV are at 4, 5, 6, 7 m distance from the origin of the calculated domain.

The segregation profiles at different cross-sections are shown in Fig. 10. At position I), just before the start of MSR, the typical 'W'-shaped segregation profile is present. In section II), located in the first half of MSR segment, the same profile shape exists but the positive peak and negative valleys become more pronounced. Position III) and IV) are located after the MSR segment. Both c_{mix} peak and valleys move downwards to below c_0. Finally, a large negative segregation in the strand core region is predicted. The deviation of c_{mix} across the slab section, Δc_{mix}, for Case 5 is 3.2 x 10^{-4} - one of the worst cases. Fig. 11 shows the evolution of c_{mix} along the casting centerline. The centerline c_{mix} increases in the first half of the MSR segment, and the positive segregation peak reaches as high as 0.19 wt.%. In the second half of the MSR segment, c_{mix} at the centerline decreases rapidly until the end of the MSR segment.

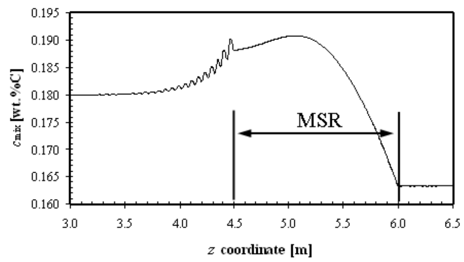

Figure 11. Evolution of the macrosegregation along the casting centerline for Case 5.

5.3. MSR segment without volume compression or tension (Case 4)

For the Case 4, the same reduction rate as previous cases is applied, but γ is equal to 0, indicating that no volume compression or tension is applied to the MSR segment. The main flow mechanism in the MSR segment happens in order to compensate the solidification shrinkage.

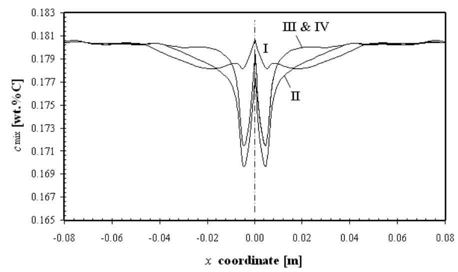

Figure 12. Predicted macrosegregation distribution profiles across different cross-sections for Case 4. The cross sections I, II, III, IV are 4, 5, 6, 7 m from the origin of the calculation domains.

The interdendritic flow pattern of Case 4 is similar to the Case 3, but the magnitude of velocity is similar to Case 1, where no MSR is applied. The finally predicted macrosegregation profile is shown with curve IV) in Fig. 12. Coincidently, the peak value of the 'W'-curve of c_{mix} is equal to the nominal composition of the alloy c_0. The c_{mix} value at the two valleys is 17.2 x 10^{-4}. The deviation of c_{mix} across the slab section, Δc_{mix}, for Case 4 is 0.8 x 10^{-4}, a good and satisfactory result. Fig. 13 shows the evolution of the macrosegregation along the casting centerline. In the first part of the MSR segment c_{mix} is significantly reduced, and negative centerline segregation is obtained. Starting from around 5.1 m, c_{mix} at the centerline tends to increase again. At the end of MSR, c_{mix} reaches almost c_0.

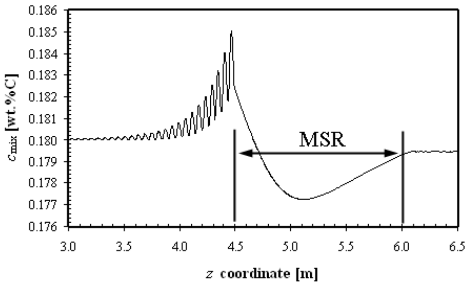

Figure 13. Evolution of the macrosegregation along the casting centerline for Case 4.

5.4. Influence of MSR position (Case 7 vs. Case 3)

As seen in Table 2, almost all MSR parameters for Case 7 are the same as for Case 3 except for the start point of the MSR segment, which is changed from $f_{\mathrm{s,Start}}^{\mathrm{cent}}$ =0.4 for Case 3 to 0.2 for Case 7. The flow patterns for both cases are quite similar except for the velocity magnitude in the second half of MSR segment. For Case 7, the predicted magnitude of $|\Delta\vec{u}_{\ell-\mathrm{s}}|$ at 5.94 m from the origin is 1.0 x 10^{-4} m·s^{-1}, while that for Case 3 is only 2.0 x 10^{-5} m·s^{-1}. The maximum $|\Delta u_{x,\ell-\mathrm{s}}|$ is 7.0 x 10^{-6} m·s^{-1}, which is similar to Case 3 (5.0 x 10^{-6} m·s^{-1}). The relatively large $|\Delta\vec{u}_{\ell-\mathrm{s}}|$ near the end of the MSR segment for Case 7 is due to feeding of the solidification shrinkage of a relatively large downstream region where solidification still continues.

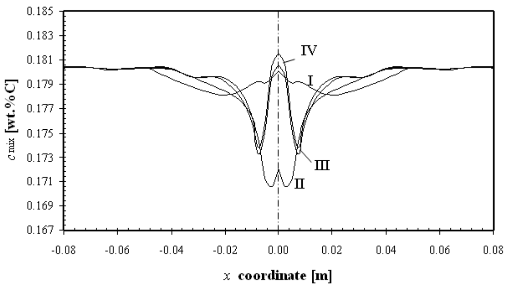

Figure 14. Predicted macrosegregation distribution profiles across different cross-sections for Case 7. The cross sections I, II, III, IV are 4, 5, 6, 7 m from the origin of the calculation domains.

As shown in Fig. 14-15, the variation of c_{mix} across the slab section or along the casting centerline for the Case 7 is quite similar to the Case 3 (Fig. 7-8). The major difference occurs in the second half of MSR. Normally in the second half of MSR, both values of the c_{mix} peak and valleys increase. However, the increase of c_{mix} for Case 7 is significantly smaller than that for Case 3. Finally, a relatively small segregation peak accompanied by two mild negative segregation valleys is achieved. The deviation of c_{mix} across the slab section, Δc_{mix}, for Case 7 is only 8.0 x 10^{-5}, much better than for Case 3, for which Δc_{mix} is predicted 1.5 x 10^{-4}.

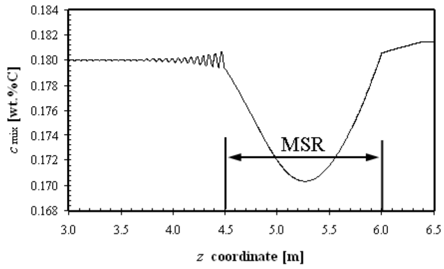

Figure 15. Evolution of the macrosegregation along the casting centerline for Case 7.

5.5 Flattening (Case 8 to 12)

A simple anti-bulging idea is proposed to compensate the centerline segregation: 'flattening' the slab surface during the late stage of solidification. Starting from a certain position, the slab surface between roll-pairs is flattened out. It might be quite challenging or unrealistic to put this idea into operation. However, the numerical study might help to improve the understanding of MSR. Flattening can also be considered as a special case of MSR that's no bulging, ε set to zero, and $u_{z,\mathrm{s}}^{\mathrm{IN}} = u_{z,\mathrm{s}}^{\mathrm{OUT}}$.

Five simulations were performed, Case 8 through 12. The starting point of flattening is fixed at 4.5 m from the origin. A so-called modified heat capacity method [15] was used to adjust the crater end position. In each simulation case, only a portion of solidification latent heat Δh_{f} is accounted for. This treatment facilitates the numerical parameter study to vary the crater end position while keeping the other casting boundary conditions unchanged. For example, in Case 8 when 65% of latent heat Δh_{f} is accounted for, the f_{s} = 0.5 isoline ends at the starting point of flattening. In Case 12 when 100% of Δh_{f} is accounted for, the f_{s} = 0.01 isoline ends at the starting point of flattening.

The corresponding simulation results are summarized in Fig. 16-17 and in Table 2. In Case 8, where flattening starts at $f_{\mathrm{s,Start}}^{\mathrm{cent}}$ = 0.5, the peak c_{mix} at the slab center reaches a level of 18.7 x 10^{-4}, while the minimum c_{mix} at the valleys is only at 16.7 x 10^{-4}. The segregation deviation Δc_{mix} is quite large (2.2 x 10^{-4}). When flattening starts at $f_{\mathrm{s,Start}}^{\mathrm{cent}}$ less than 0.4, $\Delta c_{\mathrm{mix}} \le 0.8$ x 10^{-4} is predicted. This study indicates that a too late flattening will degrade its efficiency. Before flattening starts a positive centerline segregation is developed periodically due to the bulging-induced 'pumping' flow (Fig. 17). It seems that as f_{s} at the casting center is less than 0.4 the positive centerline segregation which formed prior to flattening is not so severe. If the bulging is suppressed afterwards by flattening, the core region of the slab will solidify continuously with feeding as the only mechanism for the interdendritic flow. Feeding flow tends to reduce centerline c_{mix}. Therefore, the positive segregation developed before flattening can be partly compensated. However, when flattening starts too early ($f_{\mathrm{s,Start}}^{\mathrm{cent}} \le 0.1$), e.g. Case 11 and 12, a relatively large negative segregation zone near the casting center (Fig. 16) is predicted, although Δc_{mix} is small (0.6).

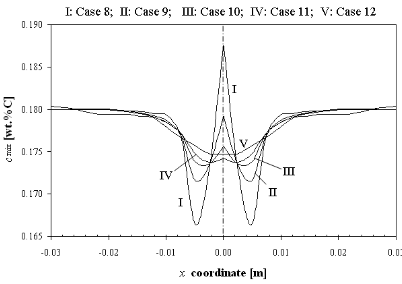

Figure 16. Final macrosegregation profiles at the outlet section of the slab. Flattening is assumed to start at different centerline solid fraction corresponding to Case 8 to 12.

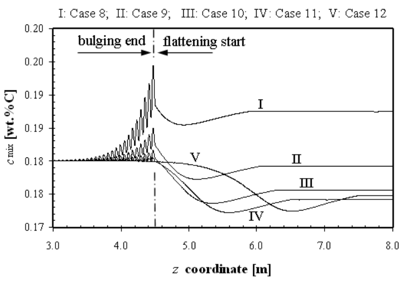

Figure 17. Macrosegregation evolution along the casting centerline. Flattening is assumed to start at different centerline solid fraction corresponding to Case 8 to 12.

6. Discussions

6.1 Principle of MSR

For a steady state situation, the centerline segregation in slab casting caused by bulging can be analyzed by the following equation:

$$\vec{u}_{\mathrm{s}} \cdot \nabla c_{\mathrm{mix}} = -f_\ell \Delta\vec{u}_{\ell-\mathrm{s}} \cdot \nabla c_\ell + f_{\mathrm{s}} (c_\ell - c_{\mathrm{s}}) \nabla \cdot \vec{u}_{\mathrm{s}} \,. \qquad (10)$$

Above equation is derived from the mass and species conservations with an assumption that the liquid and solid have the same and constant density. The error caused by this assumption is analyzed later in Fig. 18(d), where the difference between the LHS term of Eq. (10) and the sum of RHS terms is shown. This difference is relatively small. The contribution of shrinkage-induced flow to the centerline segregation becomes small in the presence of bulging and MSR-induced flow.

The LHS term of Eq. (10), $\vec{u}_{\mathrm{s}} \cdot \nabla c_{\mathrm{mix}}$, corresponds to the time derivative of c_{mix}, dc_{mix}/dt, in the Lagrangian frame referring to the moving solid phase. Time-integration of the LHS over the all volume elements along the slab centerline ($c_0 + \sum(\vec{u}_{\mathrm{s}} \cdot \nabla c_{\mathrm{mix}} \cdot \delta t)$) results in the c_{mix} profile along the centerline. Here δt is the time step required for the solid dendrites passing through each volume element. Example of the time integral of the LHS term for Case 3 is shown in Fig. 18(a). The resulting curve reproduces exactly the $c_{\mathrm{mix}} - z$ profile as simulated by the numerical model, Fig. 8.

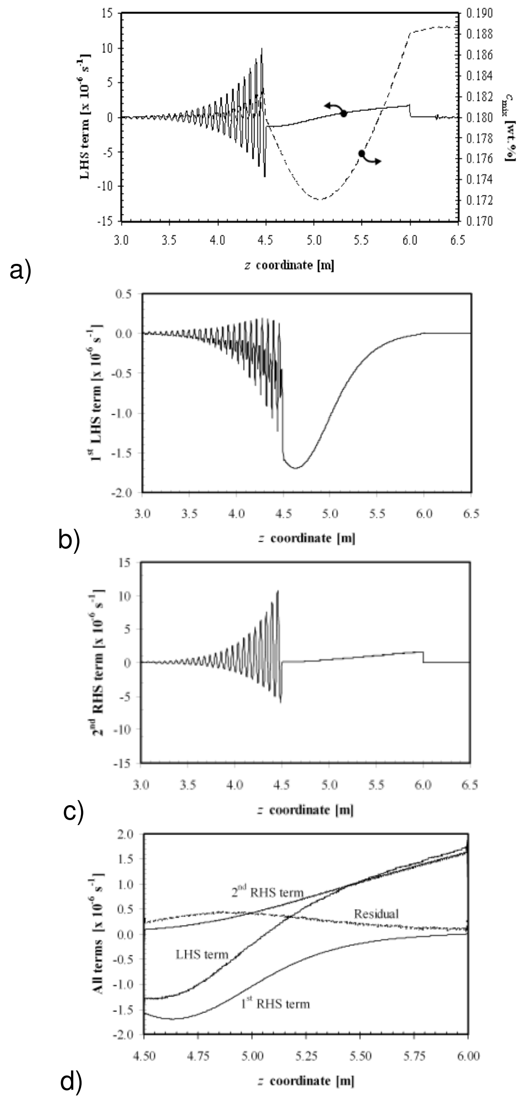

Figure 18. Formation of centerline segregation for Case 3. a) Plot of LHS term of Eq. (10) in solid line, shown together with the time-integral of the LHS term in dash line; b) Plot of 1st RHS term of Eq. (10); c) Plot of 2nd RHS term of Eq. (10); d) Comparison of the contributions of all terms (solid lines) together with the residual between the LHS term and the sum of RHS terms (dash line).

The principle of MSR to modify the centerline segregation is attributed to two parts, which correspond to the contributions of the two RHS terms of Eq. (10), i.e. ($-f_\ell \Delta\vec{u}_{\ell-\mathrm{s}} \cdot \nabla c_\ell$) and ($f_{\mathrm{s}}(c_\ell - c_{\mathrm{s}}) \nabla \cdot \vec{u}_{\mathrm{s}}$). The 1st RHS term calculates the macrosegregation caused by the MSR-induced interdendritic flow ($\Delta\vec{u}_{\ell-\mathrm{s}}$), in which a concentration gradient (∇c_ℓ) exists. A flow in direction of ∇c_ℓ, which corresponds to the situation that the higher-segregated melt is replaced by the less-segregated melt, leads to a reduction of c_{mix}. A flow in opposite direction of ∇c_ℓ which corresponds to the situation that the less-segregated melt is replaced by the higher-segregated melt, leads to an increase of c_{mix}.

The 2nd RHS term calculates the segregation caused by the non-divergence-free deforming solid phase, $\nabla \cdot \vec{u}_{\mathrm{s}} \neq 0$. For the solidification of plain carbon steel the liquid concentration of carbon (c_ℓ) is always larger than that of the solid (c_{s}). Therefore, a positive $\nabla \cdot \vec{u}_{\mathrm{s}}$ tends to increase c_{mix}, which is the case when the MSR segment is in tension ($\gamma > 0$) and the solute-enriched melt is sucked into the enlarged interdendritic areas in the MSR segment. On the contrary, a negative $\nabla \cdot \vec{u}_{\mathrm{s}}$ tends to decrease c_{mix}, which is the case when the MSR segment is compressed ($\gamma < 0$) and the solute-enriched interdendritic melt is squeezed out of the segment.

As detailed in Fig. 18, for Case 3 all three terms of Eq. (10) had been calculated and compared. The MSR segment is in tension, $\gamma > 0$ and $\nabla \cdot \vec{u}_{\mathrm{s}} > 0$. The contribution of the 2nd RHS term of Eq. (10) is always positive in the MSR segment and hence causes an increase of c_{mix}. The contribution of the 1st RHS term of Eq.(10) is negative, as the flow is mostly in the same direction as the concentration gradient (Fig. 6), hence causes a reduction of c_{mix}. The contribution of the 1st RHS term seems to dominate in the first half of the MSR segment, while the role of the 2nd RHS term overwhelms in the second half of the MSR segment. As the total effect, the contribution of the 2nd RHS term is much larger than the 1st RHS term, and hence positive centerline segregation is achieved in the MSR segment.

According to the current parameter study in all other cases (with exception of Case 4) the contribution of the 2nd RHS term always overwhelms the 1st RHS term. Therefore, the role of MSR can be primarily analyzed by the 2nd RHS term of Eq. (10). A MSR segment where the strand is in compression causes a decrease of c_{mix}; a MSR segment where the strand is in tension causes an increase of c_{mix}. Whether the MSR segment is tensioned or compressed is determined by γ. It is generally expected that a compression of MSR segment with γ<0 would compensate the positive centerline segregation, which is initiated by the bulging ahead of the MSR segment.

People usually think that when a certain amount of reduction (ε) is applied, the MSR will be in compression to reduce the centerline positive segregation. Unfortunately, according to Eq. (2) and the current simulation results, this is not always true. The value of γ is the outcome of ε, l_{SR}, $u_{z,\mathrm{s}}^{\mathrm{IN}}$, $u_{z,\mathrm{s}}^{\mathrm{OUT}}$. Whether the MSR segment is in compression or tension depends not only on the reduction amount (ε) in the thickness direction, but also on the deformation behavior in the longitudinal (casting) direction ($u_{z,\mathrm{s}}^{\mathrm{IN}}$, $u_{z,\mathrm{s}}^{\mathrm{OUT}}$). As seen in Table 2, by keeping the rest MSR parameters constant, γ can be varied with $u_{z,\mathrm{s}}^{\mathrm{OUT}}$.

6.2 Influencing parameters for MSR efficiency

The MSR efficiency, evaluated by Δc_{mix}, is found to strongly depend on γ. Therefore, Δc_{mix} together with the minimum and maximum c_{mix} across the casting section are plotted as function of γ in Fig. 19. We find that the best MSR efficiency is achieved when γ is about 0. This conclusion does not contradict the previous expectation that a slight compression of the MSR segment (γ<0) would produce optimal result. We know that, when γ=0, the contribution of the 2nd RHS term disappears. In this special case only the contribution of the 1st RHS term remains. As the flow pattern is significantly modified by the flattening slab surface in the MSR segment, the centerline segregation is modified through the contribution of the 1st RHS term of Eq. (10). If a Δc_{mix} of 1.0 x 10^{-4} is defined as the tolerance limit, γ should be controlled in the grey band shown in Fig. 19 between -1.2 and 2.8 x 10^{-6}.

Please note that the divergence-free (γ=0) scenario occurs when $u_{z,\mathrm{s}}^{\mathrm{IN}}$ = 0.006 m/s and $u_{z,\mathrm{s}}^{\mathrm{OUT}}$ = 0.005989 m/s, rather than that when $u_{z,\mathrm{s}}^{\mathrm{IN}} = u_{z,\mathrm{s}}^{\mathrm{OUT}}$. With $u_{z,\mathrm{s}}^{\mathrm{IN}} = u_{z,\mathrm{s}}^{\mathrm{OUT}}$, corresponding to Case 2 (Table 2), γ is equal to -7.44 x 10^{-6}, and the MSR efficiency is not optimal.

To investigate the influence of the MSR position, a comparison of Case 3 with Case 7 was made and described in Section 5.4. It is shown that an early start of MSR ($f_{\mathrm{s,Start}}^{\mathrm{cent}}$=0.2) leads to a better MSR efficiency than a late start of MSR ($f_{\mathrm{s,Start}}^{\mathrm{cent}}$=0.4). The current model did not consider bulging in the MSR segment. The reality is that when the MSR starts too early, the solidified shell in the MSR is not sufficiently strong and bulging may also occur in the MSR segment. This will to some extent degrade the MSR efficiency.

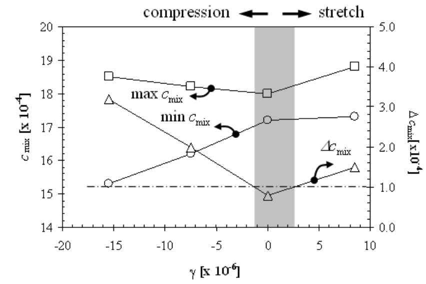

Figure 19. The calculated $\Delta c_{\mathrm{mix}} - \gamma$ map. Here the starting position of MSR is kept at $f_{\mathrm{s,Start}}^{\mathrm{cent}}$=0.4.

A further interesting phenomenon is that the flattening seems to produce better result than the MSR. This phenomenon does not actually contradict the previous studies as the positive centerline segregation in slab casting is mainly originated from bulging: In order to avoid the formation of positive centerline segregation bulging must be avoided. Flattening is adequate to achieve this goal. However, flattening must be performed in a suitable range ($f_{\mathrm{s,Start}}^{\mathrm{cent}}$ from 0.2 to 0.4) to produce satisfactory results. To implement a flattening process in industry might be difficult or even unrealistic. However, our numerical study on influencing centerline segregation by flattening implies that keeping flat strand surfaces (avoiding bulging) is more important than controlling other MSR parameters.

6.3 Model uncertainties and further improvements

No thermo-mechanical model was implemented. An exponential curve was used to describe $u_{x,s}^{b}$ for the low solid fraction zone (Eq. (1)), instead of using a linear reduction of $u_{x,s}^{b}$ [7-8]. The mushy zone within a strand behaves more likely such that most deformations occurs near the strand core where the solid volume fraction is the lowest, rather than a homogeneous deformation across the whole section of the mushy zone. This opinion has been supported by many recent experimental studies [16-18]. However, the determination of the empirical constants in Eq. (1) might be difficulty.

Industry practice has shown that pores often appear together with the centerline segregation. An argument in favour of ignoring the pore formation in our numerical model is that one of the MSR target is to suppress the pore formation. Actually, no pores are expected after an adequate MSR.

Another uncertainty regarding to the deformation in the width direction might not be so severe for slab castings as long as the width-to-thickness ratio is sufficient large [19]. Crack formation is out of the scope of our study, but it is another factor limiting the MSR operation parameters [2-3], for which attention should be paid to when the current model is applied for a real continuous process optimization.

7. Conclusions

An Eulerian two-phase columnar solidification model is used to study the principle of mechanical softreduction (MSR). A benchmark slab casting (9 m long, 0.215 m thick) of plain-carbon-steel was simulated. The main conclusions which highlight our improved understanding of the principle of MSR is summarized as follows:

1. Two mechanisms operate during MSR in order to modify the centerline segregation: one is to establish a favourable interdendritic flow field; another one is to create a non-divergence-free deformation in the mushy region. They correspond to the contributions of the two RHS terms of Eq. (10). The current benchmark study shows that the contribution of the 2nd RHS term overwhelms finally over the 1st RHS term. A MSR segment in volume compression tends to reduce positive centerline segregation; whereas a MSR segment in volume tension tends to increase positive centerline segregation.
2. A Δc_{mix} - γ map is established to empirically evaluate the MSR efficiency. The MSR factor (γ), understood as the volume averaged divergence of the solid velocity of the whole MSR segment, is defined by Eq. (2) based on ε, l_{SR}, $u_{z,s}^{\text{IN}}$ and $u_{z,s}^{\text{OUT}}$. The MSR efficiency depends not only on the reduction amount in the slab thickness direction, but also on the deformation behaviour in the longitudinal (casting) direction.
3. A numerical study on flattening, i.e. an anti-bulging process by flattening out the slab surface between roll-pairs, is made. The results imply that keeping flat surface (avoiding bulging) is more important than controlling other MSR parameters.
4. An early start of MSR or flattening seems to show better reduction efficiency than a late start. Some caution should be taken in the use of this statement, as we have not yet considered bulging in the MSR segment. This topic is currently under investigation.
5. The current model has been verified to have great application potential for a qualitative study of the MSR efficiency and its influencing parameters. However, attention should be paid when applying the model for quantitative predictions of real casting conditions. The major uncertainties are (i) the solid velocity during deformation in the slap center, (ii) ignorance of pore and crack formation, (iii) ignorance of bulging in the MSR segment and (iv) ignorance of the deformation of the slab in width direction. Further model refinements are needed.

Acknowledgement

This work is financially supported by the Austrian Christian-Doppler Research Society, voestalpine Stahl Linz, Siemens VAI Metal Technologies, and voestalpine Stahl Donawitz.

References

[1] Schwerdtfeger K.: Metallurgie des Stranggießens – Gießen und Erstarren von Stahl, Düsseldorf: Verlag Stahleisen, (1992).
[2] Thome R.; Harste K.: Steel Res. Int., 75 (2004), p. 693.
[3] Thome R.; Harste K.: ISIJ Int., 46 (2006), p.1839.
[4] Preßlinger H.; Ilie S.; Reisinger P.; Schiefermüller A.; Pissenberger A.; Parteder E.; Bernhard C.: ISIJ Int., 46(2006), p1845.
[5] Bode O.; Schwerdtfeger K.; Geck H.G.; Höfer F.: Ironmaking Steelmaking, 25(2008), p.137.
[6] Ogibayashi S.; Kobayashi M.; Yamada M.; Mukai T.: ISIJ Int., 31(1991), p.1400.
[7] Miyazawa K.; Schwerdtfeger K.: Arch. Eisenhüttenwes, 52(1981), p. 415.
[8] Kajitani T.; Drezet J.-M.; Rappaz M.: Met. Mater. Trans., 32A (2001), p. 1479.
[9] Mayer F.; Wu M.; Ludwig A.: McWASP XII, eds. Cockcroft S.L.; Maijer D.M.; TMS Publication, (2009), p. 279.
[10] Mayer F.; Wu M.; Ludwig A.: Steel Res. Int., 81(2010), p. 660.
[11] Ludwig A.; Wu M.: Mater. Sci. Eng. A, 413-414(2005), p. 109.
[12] Wu M.; Ludwig A.: Metall. Mater. Trans., 37A(2006), p.1613.
[13] Wu M.; Ludwig A.: Metall. Mater. Trans., 38A(2007), p. 1465.
[14] Ludwig A.; Grasser M.; Wu M.; Kuhn A.; Riedle J.: Fluid Dynamics Mater. Proc., 1(2006), p. 285.
[15] Niyama E.; Uchida T.; Morikawa M.; Saito S.: AFS Int. Cast Metals Res., 6(1981), p. 16.
[16] Dahle A. K.; St. John D. H.: Acta Mater., 47(1999), p. 31.

[17] Shen H.F.; Beckermann C.: Met. Mater. Trans., 33B(2002), p. 69.
[18] Nicolli L.C.; Mo A.; M'Hamdi M.: Met. Mater. Trans., 36A(2005), p. 433.
[19] Luo S.; Zhu M.; Ji C.; Yang Y.; Yang J.: J. Univ. Sci. Techn. Beijing, 32(2010), p. 890.